

HIGH-RESOLUTION SPECTROSCOPY OF MARS: RECENT RESULTS.

Vladimir Krasnopolsky, Catholic University of America, Washington, DC, USA (vkrasn@verizonmail.com).

Introduction:

The basic data on the chemical composition of Mars' atmosphere were obtained by the Viking mass spectrometers a quarter of century ago. Spacecraft missions to Mars in the last decade have not been aimed to this field, and the current progress is related to high-resolution spectroscopy.

HDO:

Deuterated water was detected by *Owen et al.* (1988) using CFHT/FTS with resolving power $\nu/\delta\nu = 9 \times 10^4$ (Fig. 1). Very low humidity (0.5 pr. mm) above Mauna Kea and a significant (by a factor of 6) enrichment of water in D on Mars facilitated the detection.

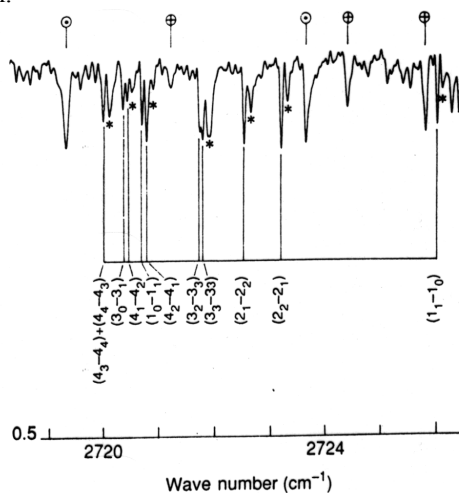


Fig. 1. HDO lines in the CFHT/FTS spectrum. Telluric HDO (*), CH₄ (+), and solar (○) lines are also seen.

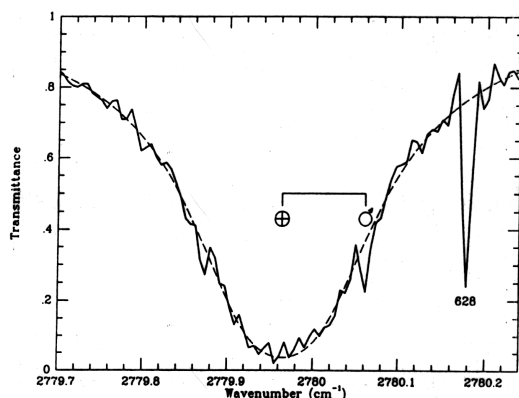


Fig. 2. One of ten HDO lines in the KPNO/FTS spectrum. Telluric line is much stronger and broader than the Martian line. Dashed curve is a model fit to the telluric line, 628 is the CO¹⁸O line.

Ten HDO lines in the KPNO/FTS spectrum (*Krasnopolsky et al.* 1997) were also used to meas-

ure the D/H ratio in water on Mars (Fig. 2). Despite the better spectral resolution ($\nu/\delta\nu = 2.7 \times 10^5$), the HDO lines were less prominent because of the much higher humidity (14 pr. mm) above Kitt Peak. Both observations agree and result in $D/H = 5.5 \pm 1$ times the terrestrial value in the Martian water. The KAO observation of HDO (*Bjoraker et al.* 1989) is still under revision.

Atomic Deuterium:

The D Lyman- α line at 1215.34 Å is shifted from the H line by 0.33 Å and very much weaker than the H line. The Martian lines are Doppler-shifted by 0.06 Å maximum relative to the telluric lines. All four lines were detected and resolved (Fig. 3) in the HST/GHRS observation (*Krasnopolsky et al.* 1998). The instrument resolving power was 1.6×10^4 . The observed D-line intensity of 23 ± 6 R at solar minimum corresponds to $[D] = 450 \pm 120 \text{ cm}^{-3}$ at 250 km.

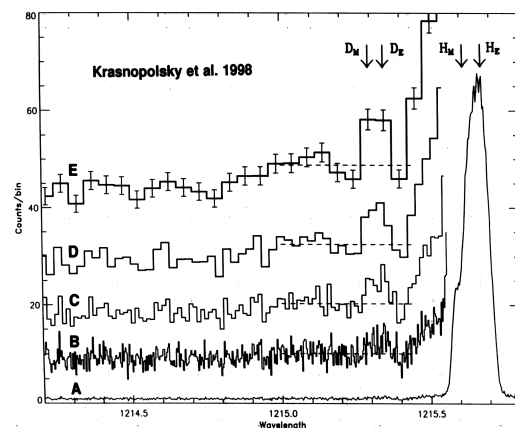


Fig. 3. Telluric and Martian (subscripts E and M, respectively) Lyman- α lines of H and D in the HST/GHRS spectrum at five levels of binning.

Molecular Hydrogen:

Vibrational and rotational transitions are strongly forbidden in H₂. Despite the low dissociation energy of 4.48 eV, dissociation to the ground-state H atoms is parity-forbidden, and H₂ absorbs photons only below 1108 Å where the solar radiation is weak. Therefore detection of H₂ presents a difficult problem. Fortunately, three absorption lines of H₂ coincide with the strong solar Lyman β , γ , and C II lines and originate a few comparatively strong emission lines. These lines were observable (Fig. 4) in the FUSE spectrum of Mars (*Krasnopolsky and Feldman* 2001). The observation resulted in a column H₂ abundance of $(1.71 \pm 0.13) \times 10^{13} \text{ cm}^{-2}$ above 140 km. The FUSE spectrum of Mars (*Krasnopolsky*

and Feldman 2002) covered a range of 904 to 1186 Å with spectral resolution of 0.2 Å. The spectrum is of high quality and provides a detection limit of ≈ 0.1 R. Many Martian lines and ion species N^+ , C^+ , and Ar^+ have been observed for the first time in that spectrum. For example, two Ar^+ and eight H lines of the Lyman series are among other lines in Fig. 5.

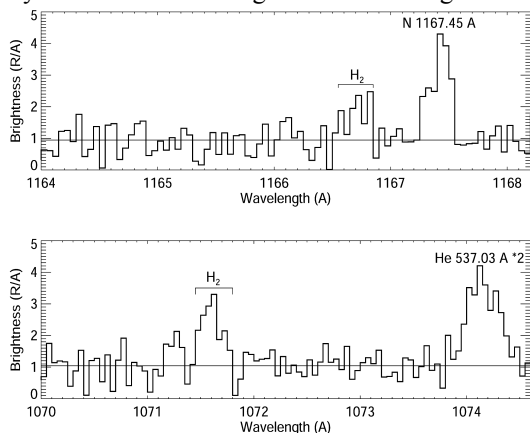


Fig. 4. Fragments of the FUSE spectrum near the H_2 lines at 1166.76 and 1071.62 Å.

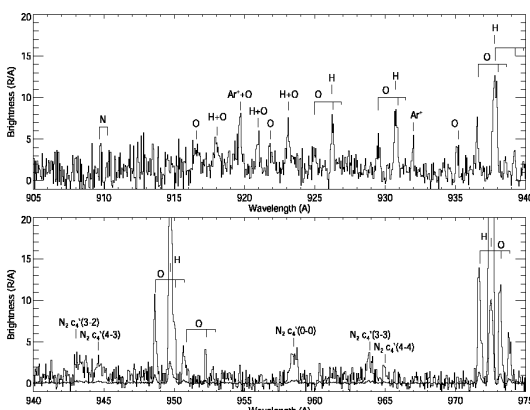


Fig. 5. A part of the FUSE spectrum.

Interpretation of the Observed HDO, D, and H_2 :

Detailed photochemical modeling of Mars' upper atmosphere and ionosphere (Krasnopolsky 2003a) to fit the observed D and H_2 abundances results in the HD and H_2 mixing ratios of 11 ± 4 ppb and 15 ± 5 ppm, respectively. Then

$$R = \frac{HD / H_2}{HDO / H_2O} = 0.4.$$

This agrees with the fractionation of D in chemical reactions ($R \approx 1.6$, Yung *et al.* (1988)), photolysis of H_2O ($R \approx 0.4$, Cheng *et al.* 1999), and the HDO depletion above the condensation level ($R \approx 0.7$, Fouchet and Lellouch 2000, Krasnopolsky 2000). Finally, $R = 1.6 \times 0.4 \times 0.7 \approx 0.4$, and the controversial problem of deuterium fractionation in Mars' atmosphere looks solved. The observed HDO, D, and H_2 require the escape fractionation factor

$$f = \frac{\phi_D / \phi_H}{D / H} = 0.105$$

averaged over the solar cycle.

Implications for Evolution of Water:

Combining this fractionation factor with the water abundance in the polar caps (a global-mean layer of ≈ 14 m deep, Jakosky 1990, Smith *et al.* 1999, Head 2001) and the $D/H = 1.9$ (Leshin 2000) at the end of the intense impact erosion of the atmosphere 3.8 Ga ago, this results in a loss of an ocean of water of 30 m deep for this period.

Hydrodynamic escape of H_2 released in the reaction $Fe + H_2O \rightarrow FeO + H_2$ could be effective for 0.1-0.3 Ga after Mars' formation. Using a fractionation factor of 0.8 for this escape (Zahnle *et al.* 1990) and a standard assumption of the terrestrial value for the initial D/H on Mars, the total loss of water by hydrodynamic escape was 1.2 km. Therefore Mars could initially be even more rich in water than Earth.

Helium:

Helium was detected on Mars using the EUVE/LW spectrometer (Krasnopolsky *et al.* 1994) that had a capability to detect the He 584 Å line against the strong geocoronal emission of this line. The observed line intensity of 57 ± 15 R corresponds to the He mixing ratio of 4 ± 2 ppm (Krasnopolsky and Gladstone 1996). Helium is lost from Mars mostly by electron impact ionization above the ionopause and sweeping out of the ions by the solar wind. The total loss is equal to $7 \times 10^{23} s^{-1}$ and agrees with the Phobos measurements (Barabash *et al.* 1995). A source of He on the terrestrial planets is the radioactive decay in the uranium and thorium chains with subsequent outgassing. It is similar to the outgassing of ^{40}Ar formed by the decay of potassium. A coupled model for the outgassing of He and ^{40}Ar showed that (1) outgassing from Mars is weaker than that from Earth by an order of magnitude, (2) outgassing of He from Mars covers a third of its loss. An additional source of He is required, and that should be a capture of the solar-wind α -particles with an efficiency of ≈ 0.3 . This is the first and probably the only case when a capture of the solar wind is critical to a balance of atmospheric species. Later calculations of the solar wind capture efficiency by Mars (Brecht 1997) confirmed our conclusion and also gave the value of 0.3 for α -particles.

Ozone and O_2 1.27 μm Dayglow:

Ozone is a tracer of Mars photochemistry, and a latitudinal-versus-season mapping of O_3 , similar to that done for H_2O by the Viking/MAWD (Jakosky and Farmer 1982) and MGS/TES (Smith 2002), is the objective of ozone observations. Three tools are currently used. Infrared heterodyne spectroscopy at 9.6 μm (Espenak *et al.* 1991) gave the first data on the O_3 distribution at low and middle latitudes (Fig. 6). The instrument resolving power was 10^6 in the published observations. Another tool is the HST/FOS

UV spectroscopy near Mars' limb (*Clancy et al. 1996, 1999, Fig. 7*).

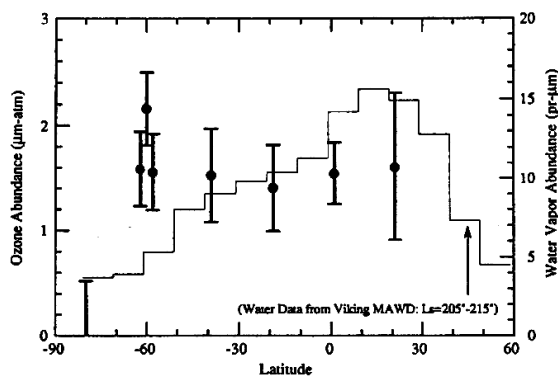


Fig. 6. Latitudinal distribution of ozone at $L_S = 208^\circ$ (*Espenak et al. 1991*).

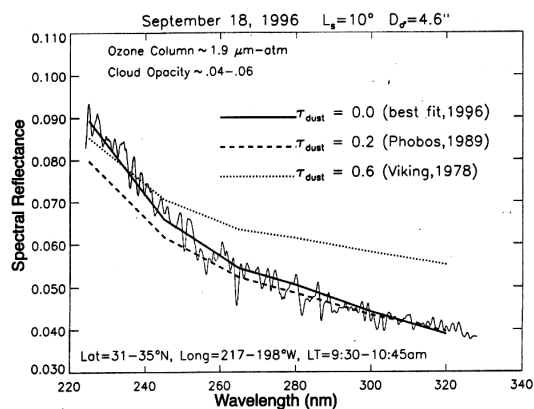


Fig. 7. Three-parameter fitting to the observed HST/FOS spectrum near Mars' limb. The parameters are ozone column and cloud and dust opacities.

According to *Clancy and Nair (1996)*, ozone above 20 km is the most sensitive to seasonal variations at low and middle latitudes. *Krasnopolsky (1997)* suggested to observe the O_2 1.27 μm dayglow using IRTF/CSHELL to map high-altitude ozone. This dayglow is excited by photolysis of O_3 and quenched by CO_2 below 15-20 km. Therefore it is the best tracer of Mars' photochemistry. The IRTF/CSHELL resolving power is 4×10^4 , that is, 7.5 km/s, and the observations are feasible for the geocentric velocity ≥ 10 km/s. The dayglow spectrum observed at $L_S = 112^\circ$ (*Krasnopolsky and Bjoraker 2000*) is shown in Fig. 8. The retrieved dayglow intensities are corrected for airmass, surface reflectivity, and the instrument point spread function. (All these corrections are of a factor of ≈ 1.5 and cannot be ignored.) Latitudinal dependences of the dayglow intensity for two seasons are shown in Fig. 9. The dayglow maps have a spatial resolution of 0.1-0.2 Mars radii. Analysis of the dayglow observation along one instrument slit was recently reported by *Novak et al. (2002)*.

CO Mixing Ratio:

Low resolution spectroscopy from the Phobos orbiter (*Rosenqvist et al. 1992*) revealed a significant (by a factor of 5-8) decrease in the CO mixing ratio above the great Martian volcanoes. This decrease contradicts to gas-phase chemistry, which predicts a constant CO mixing ratio over Mars' globe and up to ≈ 100 km. Attempts to check this result by using ground-based observations were made by *Lellouch et al. (1991)* and *Billebaud et al. (1998)* using the CO

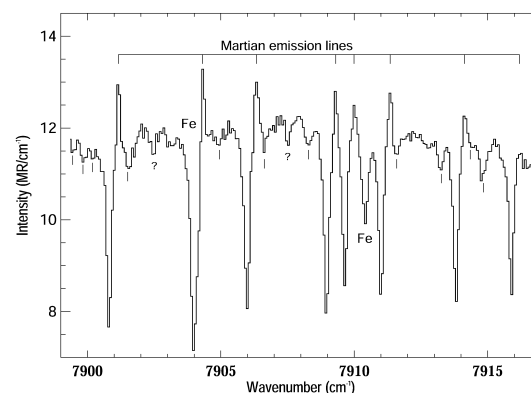


Fig. 8. One of 550 spectra of Mars observed with IRTF/CSHELL at $L_S = 112^\circ$. The main features are the telluric absorption and Martian Doppler-shifted O_2 emission lines and two solar Fe lines.

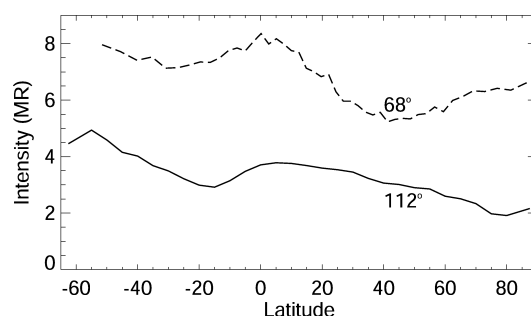


Fig. 9. Latitudinal dependences of O_2 1.27 μm dayglow at two seasons.

lines at 1.3 mm and 2.3 μm , respectively. Their fields of view were 1 and 0.5 Mars radii, respectively. No significant variations have been observed. A CO line shape at 1.3 mm (*Encrenaz et al. 1991*) also favors a CO mixing ratio, which is constant with height.

The CO mixing ratio on Mars was mapped at $L_S = 112^\circ$ (*Krasnopolsky 2003b*) by observing both CO and CO_2 lines at 1.57 μm (Fig. 10) using IRTF/CSHELL. The measured CO mixing ratio does not vary from place to place, with local time and elevation (in the range of -6 to 3 km). However, the variation with latitude is substantial (Fig. 11). It is explained by the intense condensation of CO_2 at the South (winter) polar cap. The increase in the CO mixing ratio to the South and its extent to low latitudes is determined by atmospheric dynamics. Therefore the observed latitudinal dependence as well as

similar dependences, which may be observed for all seasons throughout a whole Martian year, should be a subject of GCM simulations and provide important constraints to GCMs.

An alternative explanation of the CO increase to the South is the accumulation of CO because of the low H₂O abundance and no CO loss during the southern winter (Joshi, personal communication). However, the southern winter is shorter than the CO lifetime by a factor of ≈ 7 . Photolysis of CO₂ ceases during the polar night and is very low in the nearby regions. Therefore the expected increase in CO is smaller by an order of magnitude than that observed.

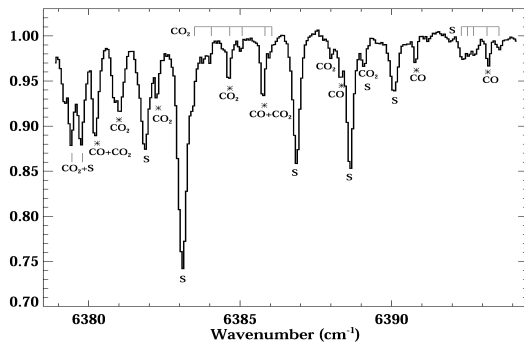


Fig. 10. One of 520 IRTF/CSHELL spectra at 1.57 μm . The spectrum consists of the CO, CO₂, and solar (S) lines.

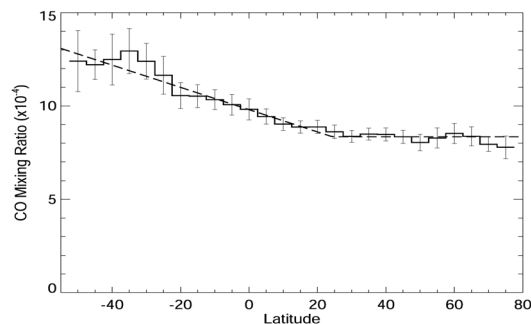


Fig. 11. Latitudinal dependence of the CO mixing ratio at $L_S = 112^\circ$.

σ

Upper Limits:

The most restrictive upper limit was obtained recently for H₂O₂ using TEXES at 8 μm . The instrument resolving power was 7×10^4 , and the limit is 3 ppb (Encrenaz *et al.* 2003), that is, below the model predictions by an order of magnitude. Upper limits of 3 ppb to HCl and H₂CO were extracted from the KPNO/FTS spectrum at 3.7 μm (Krasnopolsky *et al.* 1997). The limit to HCl shows that chlorine chemistry is negligible on Mars.

Here I do not consider very fruitful and extensive MGS/TES observations of temperature profiles, H₂O, dust and ice aerosol, and ground-based observations of water vapor.

Acknowledgment:

This work was supported by NASA Mars Data

Analysis Program (grant NAG5-10575).

References

- Barabash, S., E. Kalio, R. Lundin, H. Koskinen, *JGR* 100, 21307, 1995
- Billebaud, F., J. Rosenqvist, E. Lellouch, J. P. Maillard, T. Encrenaz, F. Hourdin, *AA* 333, 1092, 1998
- Bjoraker, G. L., M. J. Mumma, H. P. Larson, *BAAS* 21, 991, 1989
- Brecht, S. H., *JGR* 102, 11287, 1997
- Cheng, B. M., E. P. Chew, C. P. Liu, M. Bahou, Y. P. Lee, Y. L. Yung, M. F. Gershel, *GRL* 26, 3657, 1999
- Clancy, R. T., H. Nair, *JGR* 101, 12785, 1996
- Clancy, R. T., M. J. Wolf, P. B. James, E. Smith, Y. N. Bilawala, S. W. Lee, M. Calan, *JGR* 101, 12777, 1996
- Clancy, R. T., M. J. Wolf, P. B. James, *Icarus* 138, 49, 1999
- Encrenaz, T., *et al.*, *Ann. Geophys.* 9, 797, 1991
- Encrenaz, T., T. Greathouse, B. Bezard, S. K. Atreya, A. S. Wong, M. Richter, J. Lacy, *AA*, 2003
- Espenak, F., M. J. Mumma, T. Kostiuk, D. Zipoy, *Icarus* 92, 252, 1991
- Fouchet, T., E. Lellouch, *Icarus* 144, 114, 2000
- Head, J. W., *JGR* 106, 10075, 2001
- Jakosky, B. M., *JGR* 95, 1475, 1990
- Jakosky, B. M., C. B. Farmer, *JGR* 87, 2999, 1982
- Krasnopolsky, V. A., *JGR* 102, 13313, 1997
- Krasnopolsky, V. A., *Icarus* 148, 597, 2000
- Krasnopolsky, V. A., *JGR* 108, 2003a.
- Krasnopolsky, V. A., *JGR* 108, 2003b
- Krasnopolsky, V. A., G. L. Bjoraker, *JGR* 105, 20179, 2000
- Krasnopolsky, V. A., G. L. Bjoraker, M. J. Mumma, D. E. Jennings, *JGR* 102, 6525, 1997
- Krasnopolsky, V. A., S. Bowyer, S. Chakrabarti, G. R. Gladstone, J. S. McDonald, *Icarus* 109, 337, 1994
- Krasnopolsky, V. A., P. D. Feldman, *Science* 294, 1914, 2001
- Krasnopolsky, V. A., P. D. Feldman, *Icarus* 160, 2002
- Krasnopolsky, V. A., G. R. Gladstone, *JGR* 101, 15765, 1996
- Krasnopolsky, V. A., M. J. Mumma, G. R. Gladstone, *Science* 280, 1576, 1998
- Lellouch, E., G. Paubert, T. Encrenaz, *Planet. Space Sci.* 39, 219, 1991
- Leshin, L. A., *GRL* 27, 2017, 2000
- Novak, R. E., M. J. Mumma, M. A. DiSanti, N. Dello Russo, K. Magee-Sauer, *Icarus* 158, 14, 2002
- Owen, T., J. P. Maillard, C. de Bergh, B. L. Lutz, *Science* 240, 1767, 1988
- Rosenqvist, J., *et al.*, *Icarus* 98, 254, 1992
- Smith, D. E., *et al.*, *Science* 284, 1495, 1999
- Smith, M. D., *JGR* 107, 2002
- Yung, Y. L., J. S. Wen, J. P. Pinto, M. Allen, K. K. Pierce, S. Paulson, *Icarus* 76, 146, 1988
- Zahnle, K., J. F. Kasting, J. B. Pollack, *Icarus* 84, 502, 1990